Catalysis Science & Technology

CO2 Assisted Ethane Oxidative Dehydrogenation Over MoOx catalysts supported on Reducible CeO2-TiO2

Journal:	*Catalysis Science & Technology*
Manuscript ID	CY-ART-03-2021-000362.R2
Article Type:	Paper
Date Submitted by the Author:	01-Jun-2021
Complete List of Authors:	Nguyen, Thu; Rutgers The State University of New Jersey Zheng, Weiqing; University of Delaware, Department of Chemical and Biomolecular Engineering Celik, Fuat; Rutgers, The State University of New Jersey, Chemical and Biochemical Engineering Tsilomelekis, George; Rutgers The State University of New Jersey,

CO_2 Assisted Ethane Oxidative Dehydrogenation Over MoO_x catalysts supported on Reducible CeO_2-TiO_2

Received 00th January 20xx,
Accepted 00th January 20xx

DOI: 10.1039/x0xx00000x

Thu D. Nguyen[a], Weiqing Zheng[b], Fuat E. Celik[a] and George Tsilomelekis[a]**

Supported MoO_x on mixed CeO_2-TiO_2 was investigated for the oxidative dehydrogenation of ethane (ODHE) using CO_2 as a mild oxidant. Raman spectroscopic characterization of the synthesized catalysts under dehydrated conditions suggested that surface MoO_x species prefer to anchor on the crystalline domains of TiO_2. Upon increasing the amount of CeO_2 in the mixed oxide support, significant spectral changes were observed, especially in the ~900-950cm^{-1} region where Mo-O-*M* bonds are expected. The catalytic behaviors of Mo as opposed to pure support materials were distinct. As the ceria content in the support increased, MoO_x catalysts promoted oxidative dehydrogenation pathways via Mars van Krevelen mechanism while pure supports appeared to favor ethane direct dehydrogenation. Investigation of structure-function relationships via in-situ Raman spectroscopic efforts revealed that adding ceria not only changed the redox properties of the support but also improved those of the deposited amorphous MoO_x species. We also show that upon incorporation of ceria into the support, CO_2 directly participates in the reoxidation of the dispersed MoO_x species during catalysis. This effect was distinct from the participation of CO_2 in the reverse water gas shift reaction. Operando Raman spectra revealed that the presence of CO_2 prolonged the existence of the 930cm^{-1} feature which appears to correlate well with the relative contribution of oxidative versus non-oxidative pathways in ethane dehydrogenation.

Key words: Lattice oxygen, Raman Spectroscopy, Molybdena, Mixed metal oxides, ODH

Introduction

Catalytic oxidative dehydrogenation (ODH) of low molecular weight alkanes has been increasingly gaining interest as an alternative to the direct thermal dehydrogenation route[1, 2] towards the production of the corresponding olefins. Among olefins, ethylene (C_2H_4) comprises a valuable intermediate in petrochemical industry. In light of the recent shale gas revolution[3], abundant ethane (C_2H_6) resources serve as the steppingstone and strong incentive for academic and industrial communities to advance and evolve research strategies for the production of ethylene.

The requirements of modern catalytic processes for ODH of ethane demand a paradigm shift where rational design of materials directly aims to guarantee high selectivity to olefins by improving redox properties, hampering consecutive olefin overoxidation, limiting coke formation, or enhancing in-situ coke removal pathways[4]. Utilizing carbon dioxide (CO_2) as an oxidant in ODH (Eq. 1) has been recognized in recent years as a promising alternative approach that offers an attractive solution to severe total oxidation of ethylene resulting in higher selectivity to desired products[5]. Since CO_2 is the greatest contributor to global climate change, identification of selective reaction pathways in ODH involving CO_2 can potentially improve the performance of this important reaction while simultaneously reducing its carbon footprint. Besides hampering olefin overoxidation, other added benefits on the use of CO_2 in oxidative dehydrogenation routes comprise a) the in-situ release of the heat of the reaction due to the oxidation of the abstracted hydrogen[6], b) the enhanced olefin production through the shift of the equilibrium alkane conversion due to the consecutive reverse water gas shift (RWGS), c) the improved stability of catalytic materials due to CO_2 participation in coke removal mechanisms[7] and d) the potential of generating H_2/CO mixtures through dry reforming with a ratio adequate for the Fischer–Tropsch process[8, 9].

$$C_2H_6 + CO_2 \rightarrow C_2H_4 + CO + H_2O \quad (1) \quad \Delta H° = +177.6 \text{ kJ/mol (1)}$$

It is generally accepted that the alkane ODH reaction over several families of supported metal oxide catalysts is strongly dependent on the intrinsic acid-base properties and/or redox properties of the catalysts used, as well as the interaction between active sites and the support materials[10-14]. These effects have spurred research focusing on the rational engineering of catalyst supports either via doping or mixing different metal oxides with the goal of tuning the aforementioned properties in a desirable manner[10, 15, 16, 13]. Besides support effects, post-modification of these supports by depositing secondary active sites in order to improve either the selectivity to olefins or to enhance material stability in conventional ODH with O_2 (Eq.2) has also been carried out[10, 17].

$$C_2H_6 + ½O_2 \rightarrow C_2H_4 + H_2O \quad (2) \quad \Delta H° = -105.4 \text{ kJ/mol (2)}$$

However, the aforementioned effects are not clear in the case of ODH with CO_2 if one takes into account the complex reaction network that can occur simultaneously[18]. In addition, the reaction mechanism and role of CO_2 as an oxidizing agent in ODH still remains elusive. The majority of studies revealed that the oxygen assisted ODH over many classes of supported metal oxides occurs via a Mars van Krevelen (MvK)[17, 19, 20] mechanism with the participation of lattice oxygen (Eqs. 3-4).

$$C_2H_6 + M\text{–}O \rightarrow C_2H_4 + H_2O + M\text{–}\nu_o \quad (3)$$

[a] *Department of Chemical and Biochemical Engineering, Rutgers, The State University of New Jersey. Email: gt241@soe.rutgers.edu*
[b] *Catalysis Center for Energy Innovation, University of Delaware, Newark, DE 19716, USA*

Electronic Supplementary Information (ESI) available: See DOI: 10.1039/x0xx00000x

$$\mathrm{M}\text{–}\nu_{\mathrm{o}} + \frac{1}{2}\mathrm{O}_2 \rightarrow \mathrm{M}\text{–}\mathrm{O} \quad (4)$$

On the other hand, many reports concerning CO_2 assisted ODH have demonstrated the combination of direct dehydrogenation (DH) (Eq. 5) and reverse water shift (RWGS) (Eq. 6)[21, 15, 18, 22, 23] as the primary reaction pathways.

$$\mathrm{C_2H_6} \rightarrow \mathrm{C_2H_4} + \mathrm{H_2} \quad (5) \qquad \Delta H° = +136.4 \text{ kJ/mol}$$

$$\mathrm{CO_2} + \mathrm{H_2} \leftrightarrow \mathrm{CO} + \mathrm{H_2O} \quad (6) \qquad \Delta H° = +41.2 \text{ kJ/mol}$$

Additionally, in-situ coke removal via reverse Boudouard[21, 24, 22] mechanism (Eq. 7) and catalyst re-oxidation by CO_2 splittin[21, 25]g (Eq. 8) have also been proposed to address i) the complex reaction network and ii) the role of CO_2 in promoting catalyst stability.

$$\mathrm{CO_2} + \mathrm{C} \rightarrow 2\mathrm{CO} \quad (7) \qquad \Delta H° = -544.2 \text{ kJ/mol}$$

$$\mathrm{M}\text{–}\nu_{\mathrm{o}} + \mathrm{CO_2} \rightarrow \mathrm{M}\text{–}\mathrm{O} + \mathrm{CO} \quad (8)$$

However, the dearth of concrete evidence about the different reaction pathways occurring simultaneously in CO_2-assisted ODH over a wide-range of catalyst materials hinders our ability to establish a directional methodology for material improvement at the molecular level.

Among investigated catalysts, dispersed metal oxides such as MoO_x, WO_x, VO_x etc., supported on TiO_2[11, 14] have been highlighted to be catalytically active materials for C-H activation, which is the rate limiting step in ODH of ethane. In addition, the physicochemical properties of TiO_2 can be modified via the incorporation of CeO_2[26-28]. It is also noteworthy to mention that mixed CeO_2-TiO_2 supports have shown improved reactivity in other selective oxidation reactions such as the oxidation of dicloroethane[29]. In this work, we study the performance of ODH of ethane over MoO_x deposited on TiO_2 and mixed CeO_2-TiO_2 supports. This study focuses on unraveling the effect of MoO_x loading as well as nature of the composition of mixed CeO_2-TiO_2 support on the CO_2-assisted ODH of ethane. Efforts are made to understand possible competing ethane conversion pathways and how CO_2 affects the relative performance of different catalysts. In-situ and Operando Raman spectroscopy is utilized in an attempt to develop novel structure-reactivity correlations.

Experimental

Materials and synthesis of catalysts

$Ce(NO_3)_3.6H_2O$ (99.99%), $Ti(OCH_2CH_2CH_2CH_3)_4$ (97%), TiO_2 (99.9% Degussa P25), $(NH_4)_6Mo_7O_{24}.4H_2O$ (99.98%) were purchased from Evonik. Mixed CeO_2-TiO_2 was synthesized by following a sol-gel method as reported elshewhere[30, 29]. In the sol-gel synthesis, typically, solution A was prepared by vigorously stirring a mixture of 10 g $Ti(OC_4H_9)_4$, 3 mL of CH_3COOH and 40 mL of C_2H_5OH. The pH of the solution was then adjusted to 2-3 via dropwise addition of HNO_3. For solution B, an amount of $Ce(NO_3)_3.6H_2O$ was dissolved in 4 mL of deionized H_2O and 20 mL of C_2H_5OH. Solution B was then added dropwise into solution A under vigorous stirring to form a transparent, homogeneous solution. The resulting solution was aged at room temperature for 1 hr and then was heated up to 70 °C where was kept for 2 hrs in order to form a gel. The concentration of solution B was varied to modify the Ce content of the final material. The gel was dried at 70 °C for 72 hrs and the remaining solid underwent calcination at 600 °C in the presence of 100ml/min air for 4 hrs with a ramp rate of 2 °C/min. The synthesized CeO_2-TiO_2 mixtures were labeled as xCeTi, where x was formulated as:

$$x = \frac{n_{\mathrm{Ce}}}{n_{\mathrm{Ti}}} \times 100\%$$

Molybdenum oxide speceis were deposited on P25 and mixed CeO_2-TiO_2 supports by wet impregnation. A pre-calculated amount of $(NH_4)_6Mo_7O_{24}.4H_2O$ that leads to a final atomic density within 1-5 Mo/nm^2 were dissolved in 40 mL of deionized H_2O to form a transparent solution. 1 g of the prepared oxide support was then added into the solution. This slurry mixture was then dried in a rotary evaporator at 40 °C under reduced pressure before being calcined at 600 °C for 4 hrs. The final catalysts were labeled as yMo/xCeTi.

Characterization methods

Crystallinity and phase composition of synthesized CeO_2-TiO_2 samples were analyzed by using X-Ray diffraction measurements (XRD). The analysis was carried out with a PANalytical Philips X'Pert X-Ray diffractometer equipped with a Cu-Kα source at 40 kV and 40 mA and angular incidence 2θ between 20° and 90° with 0.05° step and 2.0 s per step. Silicon was used as an external standard reference to determine any possible peak shift.

The specific surface area of the prepared oxide support was estimated through the Brunauer–Emmett–Teller (BET) method using a Quantachrome Autosorb-1 instrument. The BET measurements were carried out at cryogenic condition after degassing samples at 150 °C for 3 h.

Absorbance properties of purchased P25 and prepared CeO_2-TiO_2 were characterized using UV-vis spectroscopy. Diffuse-reflectance UV-visible spectroscopy was carried out in a Thermo Scientific Evolution 3000 spectrophotometer equipped with a Harrick Scientific Praying Mantis diffuse reflectance accessory. Spectra were scanned between 190 nm and 1100 nm in intervals of either 0.5 nm or 2.0 nm. The absolute reflectance standard was collected using a Spectralon® disk.

Raman spectroscopy studies were carried out using a HORIBA LabRAM HR Evolution high spatial and spectral resolution spectrometer. The incident beam (532 nm, 80 mW) was directed on the samples and focused by a 50x long-working distance objective. The power of the laser was maintained below 5mW at the location of the sample via neutral density filters. For the in-situ Raman measurements, the laser line was directed into a reaction cell (Harrick Scientific Products Inc.) and relevant reaction mixture flow was provided via mass flow controllers (Alicat Scientific). To further secure temperature control and ensure thermal stability, only a very thin layer of sample was loaded into the sample holder of the Harrick cell. This helped us to avoid large temperature gradient between the spot, where the thermocouple is located, and the surface of the sample. Collection of the scattered light was achieved with an

air-cooled (−75 °C) open electrode 1024 × 256 pixels CCD. The acquisition time and the total number of accumulations were varied within the 5-20 sec and 10-60 ranges respectively.

Transmission electron microscopy (TEM) images were acquired with a JEM-2010F (JEOL, Japan) transmission electron microscope equipped with a field emission gun emitter.

For the H_2-TPR measurements, 0.06 g of samples were loaded into a U-shaped reactor and pretreated with air at 600ºC to dehydrate the materials. The reactor was cooled down to 25ºC and flushed with pure Ar. The temperature of the reactor was then ramped up to 650ºC with the ramp rate of 5ºC/min under a 40 mL/min flow of 2% H_2 in Ar. The H_2 consumption during the experiment was monitored by online Cirrus 3 MKS mass spectrometer.

Catalytic studies

The catalytic performance of all synthesized materials was evaluated with a continuous gas flow system through a quartz tube reactor (4 mm ID). Typically, 200 mg catalyst was diluted with 800 mg quartz sand before being loaded into the reactor. The reactor was placed inside a resistively heated ceramic furnace with external temperature control, and the catalyst bed temperature was measured with a K-type thermocouple placed in direct contact with the catalyst bed. The complete configuration of the experimental setup used can be found in our previous work. The reactor was then heated up to 600 °C in an air flow to ensure a fully oxidized state. The reactor was then flushed with a 50 mL min^{-1} flow containing pure nitrogen in 10 minutes to ensure that no O_2 was remained in the gas lines that could affect initial time-on-stream data. A mixture of reactants, containing 5% C_2H_6, 5% CO_2, and 90% N_2, was then mixed and stabilized with by-pass before being fed into the reactor. Product analysis was performed via an in-line microGC (Agilent 490) equipped with MS5A column (CH_4, CO and H_2) and PoraPlot Q column (CO_2, C_2H_4, C_2H_6, C_3H_6, C_3H_8). Conversion of C_2H_6, selectivity to C_2H_4, and yield of C_2H_4 were calculated respectively as follows:

$$X_{C_2H_6} = \frac{F_{C_2H_6,\,in} - F_{C_2H_6,\,out}}{F_{C_2H_6,\,in}} \times 100\%$$

$$S_{C_2H_4} = \frac{F_{C_2H_4,\,out}}{F_{C_2H_6,\,in} - F_{C_2H_6,\,out}} \times 100\%$$

$$Y_{C_2H_4} = (X_{C_2H_6} \times S_{C_2H_4})/100\%$$

Results and discussion

Physicochemical characteristics and structural implications of surface species

The prepared CeO_2-TiO_2 supports were characterized via BET, Raman and UV-vis spectroscopies as well as XRD in an effort to identify the basic structural properties of pure and mixed oxides, before impregnation with the active phase; relevant results are shown in **Table S1** and **Figure S1** of the supporting information. The BET surface area analysis of xCeTi samples showed that at low CeO_2 content, a negligible difference was observed as compared to pure commercial titania (P25) while at higher CeO_2 content an increase was observed. Even though XRD and Raman characterization techniques highlight anatase as the main phase present, the visible light absorbance measured in UV-Vis spectroscopy revealed the presence of a second oxide. A closer look of the Raman and XRD results underscore that there is a gradual decrease in the crystallinity of the anatase phase in the support materials which is also responsible for the increased surface area upon increasing CeO_2. Analysis of the XRD data shows that as more ceria was incorporated into the support, the crystallite size of the anatase phase is reduced. This observation is consistent with literature data concerning CeO_2-TiO_2 mixed oxides and has been ascribed to the prevention of agglomeration of anatase by ceria[30, 27, 31, 32]. In addition, the Raman spectra of all pure mixed supports that were used did not show any vibrational bands characteristic of crystalline CeO_2 nanoparticles thus highlighting the relatively good dispersion of CeOx component in the mixed phase.

Raman spectroscopic studies of dispersed molybdena species on common oxide supports and different atomic density loadings have indicated that the MoO_x saturation capacity is around 5-6 atom/nm^2 [33]. There is a wealth of information from in-situ spectroscopic studies of supported metal oxides highlighting the importance of characterizing those catalysts

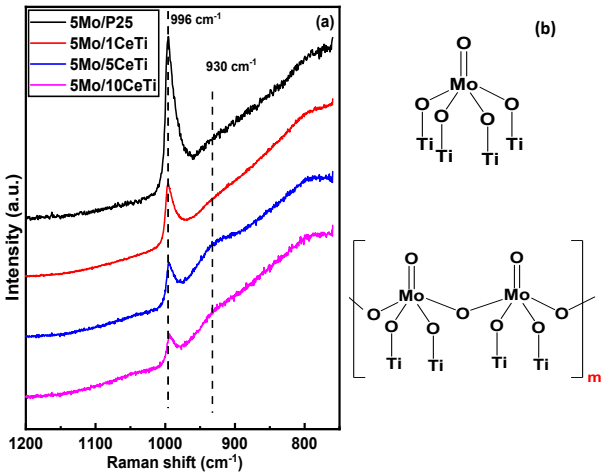

Figure 1: In-situ Raman spectra of Mo catalysts supported on different oxides under dehydrated conditions. (T=600 °C under 50cc/min of air flow. Acquisition time: 10-60 sec, Number of accumulations: 5-10)

under dehydrated conditions to simulate the structure of catalysts under reaction conditions. Since strong structural changes occur upon temperature elevation[34, 35] (i.e dehydration of surface species as well as dehydroxylation of the support[36-38]) Raman spectra of deposited molybdenum oxides under dehydrated conditions were collected at 600 °C in the presence of air as shown in **Figure 1**. The Raman spectra of **Figure 1** did not show any characteristic bands for crystalline MoO_3 indicating that the catalysts have not exceeded the monolayer coverage. However, the high temperature Raman spectra shown in **Figure 1** can suffer from strong thermal broadening and thus the presence of possible MoO_3 units may be difficult to identified. In **Figure S2**, we report low temperature Raman spectra, i.e. at 100 °C and 200 °C, of representative supported molybdena catalysts. No crystalline MoO_3 was identified since its most

intense band at ~820 cm^{-1} was absent in all catalysts. However, upon addition of Mo on the surface of the supports, the crystallite size of anatase slightly increased that is consistent with the observed surface area decrease.

The family of supported molybdena on prepared supports **Figure 1a** exhibits a distinct peak at 996 cm^{-1}. This peak represents the vibrational stretching mode of molybdenyl double bond (Mo=O)[33, 39, 38] from $(MoO_x)_n$ dispersed species (**Figure 1b**). In the open literature authors have demonstrated that on TiO_2, as loadings approaches the monolayer coverage, small polymeric Mo species can be formed; an associated shift of the Mo=O stretching mode of terminal oxygen to higher wavenumbers has been suggested[37, 40]. As more polymeric domains were formed, the band signifying mono-oxo molybdena shifted from 992 cm^{-1} to 995 cm^{-1} which is consistent with the frequencies of the stretching mode of the molybdenyl bond, shown in **Figure 1a**. This argument is further strengthened in our loading dependent study, where low (1.5Mo/nm^2) and high (5Mo/nm^2) catalysts on P25 have been characterized via Raman (**Figure S3**). A slight shift from 993 cm^{-1} to 995 cm^{-1} is also observed which substantiates the hypothesis of possible oligomeric Mo species to be present on P25 at high loadings.

Interestingly, a broad band at ~930 cm^{-1}, which was, however, insignificant in 5Mo/P25 and 5Mo/1CeTi, appeared to be strong in 5Mo/5CeTi and 5Mo/10CeTi catalysts. The assignment of this vibrational band has been debated in the open literature due to its inherent connection to catalytic reactivity implications. This band has been previously assigned in various characterization studies[33, 41, 36, 42-44, 39, 45, 35, 46-49, 38] to the Mo–O–Mo functionalities of larger $(MoO_x)_n$ polymeric domains of the dispersed phase. However, it is worth mentioning here that recent DFT and experimental[50, 51] studies on similar oxides (VO_x and MoO_x based) have shown that this band might arise also from contributions of anchoring bonds with the support, Mo-O-support, either from monomeric or oligomeric species. More details were also provided by a multiwavelength Raman approach on well controlled MoO_3/Al_2O_3 via the ALD and/or impregnation synthesis methods where a broad band spanning the 850–950 cm^{-1} (present also at low concentrations where no polymers are unlikely to be formed) was assigned to either Mo-O-Mo or more likely to Mo-O-Al. At higher loading though, there was a clear increase in a band located at 946cm^{-1} that was distinctly assigned to the Mo–O–Mo asymmetric stretch, probably of amorphous three-dimensional clusters, but not MoO_3. In our loading dependent study of the molybdenum catalysts on 5CeTi support (**Figure S3**), a similar increasing behavior in the intensity of the 930cm^{-1} was observed, supporting the argument of larger contribution of Mo-O-Mo functionalities to this vibrational band. In the case of P25, increasing molybdenum content led to a slight increase in a broad feature around 920-930cm^{-1} that can be associated with a smaller degree of oligomeric units at 600°C. A recent preprint[52] shows by means of high resolution imaging that although oligomeric (MoOx)n species may be present at room temperature on the surface of TiO_2, they undergo gradual dissociation at higher temperatures resulting at larger extent of monomeric units. This observation leads to the hypothesis that the presence of CeO_2 in the TiO_2 lattice may be responsible for the formation of larger Mo clusters on the catalyst surface.

To provide more insights into this hypothesis, in situ DRIFTS spectra have been acquired for the CeO_2-TiO_2 mixed oxides as well as the monolayer Mo based catalyst on 5CeTi support. Relevant results are shown in **Figure 2**. Based on the available reported studies in literature[53-56], bands at 3642, 3695, 3673, 3718, and 3730 cm^{-1} are assigned to hydroxyl groups present on TiO_2 surface while bands at 3634, 3650, 3663, and 3688 could be assigned to hydroxyl groups on CeO_2 surface. When Mo was deposited on the surface of the mixed oxide support, most of bands originating from -OH groups on titania surface, including the strongest band at 3718 cm^{-1}, were absent in DRIFT spectra, while many bands of OH group from ceria including one strongest band at 3634 cm^{-1} could still be detected; however, some titration of Ce-OH group is present as well highlighting the possible anchoring of Mo species to Ce sites but at much lower extent. This selective titration of the TiO_2 -OH groups on the surface of mixed oxide supports upon Mo addition in conjunction with the Raman and XRD results discussed above, suggests that dispersed amorphous MoO_x units preferentially

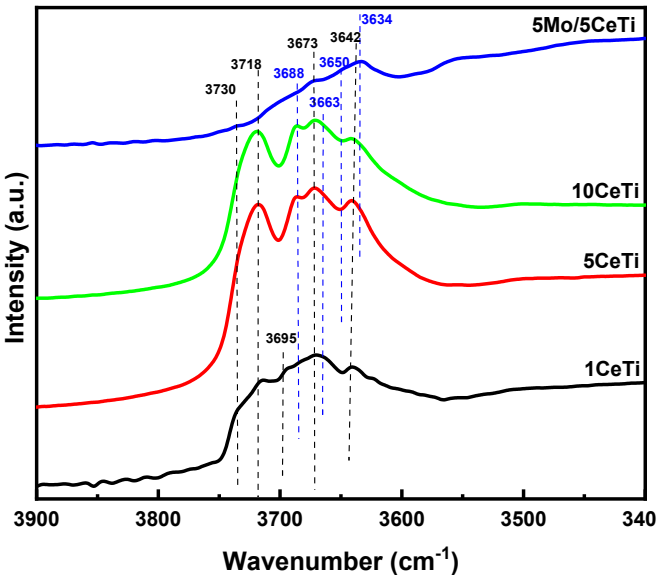

Figure 2: DRIFTS spectra of 1CeTi, 5CeTi, 10CeTi, and 5Mo/5CeTi after dehydration at 450 °C and quenched to 25 °C

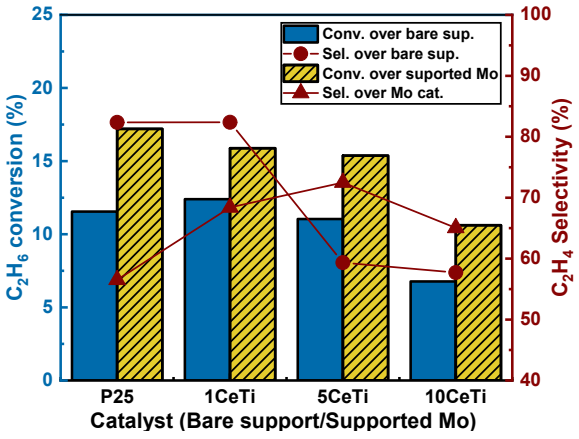

Figure 3: Initial conversion ethane and selectivity to ethylene over molybdenum oxide on different supports at 600 °C, under a 20 mL flow containing 5% C_2H_6 , 5% CO_2, and 90% N_2

(although not exclusively) anchor on the crystalline domains of TiO_2. When ceria is dispersed into the support, the crystallite size and overall crystallinity of anatase TiO_2 shrinks, thus leaving less free anatase surface area for molybdena to be anchored which in turn promotes the formation of polymeric species. The possibility that changes in crystallinity upon CeO_2 addition might also affect the dominant exposed facets thus promoting the formation of larger polymeric species with different apparent degrees of polymerization cannot be excluded. However, further studies via advanced microscopy characterization can provide invaluable insights into this research aspect.

Catalytic performance of supported MoO_x systems and competing C_2H_6 conversion pathways

Preceding any discussion of the catalytic behavior of our supported catalysts, it is important to briefly discuss the catalytic reactivity of the bare supports, summarized in **Figure 3** and supporting information. P25 exhibited 11.5% ethane conversion with an initial ethylene selectivity of 82%. The addition of a small amount CeO_2 in the mixed 1CeTi support did not cause any significant changes as compared to P25. Upon further increase of CeO_2 content in the mixed support, both ethane conversion and ethylene selectivity decreased. This decrease is correlated with the decrease in TiO_2 crystallinity observed by XRD and Raman with increased ceria content. Ceria may also be blocking some ethane dehydrogenation sites on the TiO_2 surface while simultaneously altering the crystallinity, thus fewer active sites are present. It should be noted that other studies have shown an increase in reducibility when small ceria particles are dispersed in a mixed oxide system[57], and especially in TiO_2 based systems[58]. Furthermore, when ceria was used as a modifier and oxygen buffer, alkane overoxidation was enhanced[59]. As the loss of ethylene selectivity was due to overoxidation to CO and CO_2, the enhanced oxygen storage and oxygen mobility in high ceria loadings can explain the drop in selectivity.

The addition of dispersed MoO_x on the surface of all catalyst supports was evaluated and relevant results regarding their catalytic performance are also depicted in **Figure 3**. Since no crystalline MoO_3 was identified, any changes observed in the catalytic reactivity solely depend on the contribution of the amorphous MoO_x units. The addition of molybdenum oxide enhanced the initial ethane conversion as compared to all bare supports. This underscores that the presence of MoO_x reactive sites on supports contributes to the excess ethane conversion. The initial selectivity to the desired olefin appeared to change with increasing CeO_2 content in the support and a maximum selectivity to ethylene of 72% was measured for the 5Mo/5CeTi catalyst.

Due the existence of multiple proposed dehydrogenation mechanisms on metal oxide catalysts, the influence of each catalyst active site on the flux through difference reaction pathways in CO_2-assisted ODH is complex. Oxidative dehydrogenation pathway leads to water as a product (e.g. Reaction 1), while pure dehydrogenation leads to H_2 as a product (Reaction 3)[18, 25, 22, 13, 60]. However, the amount of hydrogen in the reactor effluent is also influenced by the extent of reverse water-gas shift due to the presence of CO_2 in the feed (Reaction 4). Therefore, the relative amount of different species in the effluent can offer clues for the dominant pathways in play over a given catalyst, or during specific reaction conditions.

An added complication is that the oxidation state of the catalyst and/or support may vary as the reaction proceeds. For this reason, the initial reactivity, when the catalyst is still fully oxidized, can give insights into the intrinsic competitive behavior between direct dehydrogenation (DH) and ODH of ethane at the same active sites. Both the ethane and CO_2 conversion are lower than the anticipated conversion as predicted from thermodynamic calculations[6] underscoring that the results presented herein are far away from thermodynamic equilibrium. The fact that the CO_2 conversion achieved in our experiments is low can help to establish a methodology for disentangling plausible simultaneous pathways for olefin production. At sufficiently low CO_2 conversion (<5%) the extent of H_2 consumption via RWGS is limited, so the ratio of hydrogen to ethylene in the reactor effluent can serve as an indicator for the relative contribution of DH and ODH of ethane reaction pathways. The CO_2 conversion was very low within the first hour of time-on-stream, so initial rate data were suitable for this comparison. The ratio γ[61], is defined at the reactor outlet as:

$$\gamma = \frac{\text{molar flow rate of } H_2}{\text{molar flow rate of } C_2H_4}$$

In the case where direct dehydrogenation (Reaction 3) is the sole contributor to olefin formation, this ratio is expected to have a value equal to one. If one allows for additional side reactions such as C-C cracking or combustion of the olefin, the value may even exceed one. In contrast, the MvK mechanism for ODH (Reactions 1-2) alone, would result in a ratio equal to zero. Very recently, a similar ratio (namely F_{tandem}) by Stair and Notestein was introduced to explain the possibility of tandem H_2 combustion in propane dehydrogenation[62].

Figure 4 depicts the effect of CeO_2 addition on the γ ratio at early reaction times. Comparing the performance of the bare supports, it is observed that γ ratio slightly increases with higher ceria content. This behavior indicates either higher direct

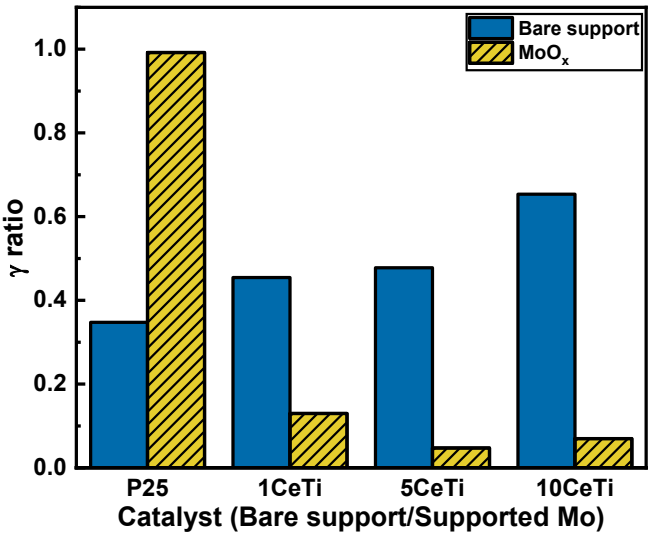

Figure 4: Initial ratio of produced H_2 to produced C_2H_4 over 5Mo/xCeTi at 600 °C under a flow of 20 mL/min containing 5% C_2H_6, 5% CO_2 and 90% N_2

dehydrogenation activity and/or the presence of side reactions such as overoxidation/combustion (see Table S3).

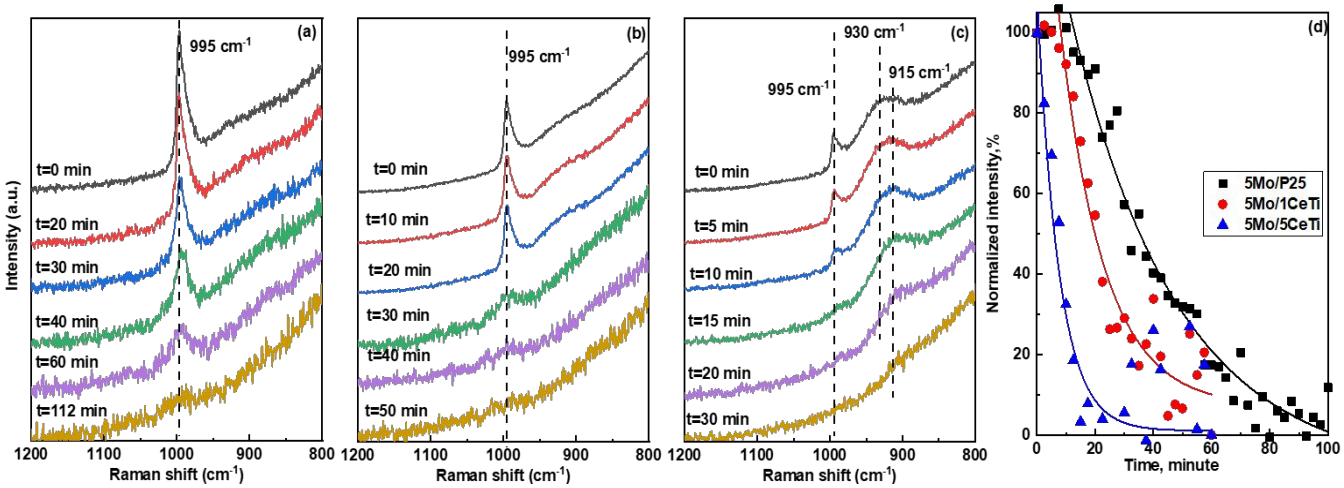

Figure 5: In-situ Raman spectra of reduction over (a) 5Mo/P25, (b) 5Mo/1CeTi, (c) 5Mo/5CeTi at 600°C under a 50mL/min flow containing 0.5 % H_2, and 99.5 % N_2. (d) Normalized intensity change of Mo=O peak

In the case of Mo catalysts, the initial **γ** ratio of Mo/P25 was approximately 1 that, according to the definition of **γ** ratio above, implies that ethane conversion may occur mainly through direct dehydrogenation. However, it is worth mentioning here that although the use of γ ratio is to address competitive pathways, its value can be affected from the molar flow of both H_2 and olefin. In the case of consecutive reactions, such as olefin overoxidation/combustion, the apparent value of the γ ratio will be affected by the intrinsic reactivity of the active sites towards the competitive combustion. For molybdena catalysts supported on pure TiO_2, it has been previously shown that significant olefin overoxidation hampers the overall ethylene selectivity. This observation is also responsible for the increased value of the γ ratio for the Mo/P25 catalyst presented in this work, as compared to the bare P25.

On the other hand, when molybdena was deposited on the mixed CeO_2-TiO_2, the initial **γ** ratio dropped significantly to a value of ~0.1 and varied little with CeO_2 content. This significant shift indicated very low direct dehydrogenation and implies that all, or nearly all, of the ethane conversion occurs via oxidative dehydrogenation routes, once CeO_2 is introduced into the support. The effect of COx on the γ ratio of molybdena catalysts on CeO_2-TiO_2 is minimal considering the almost constant selectivity to CO_x at similar ethane conversion. More specifically, for the case of 5CeTi supports, a Mo loading dependent study (see **Figure S4** of the supporting information) shows that this shift in the **γ ratio** is observed even at very low Mo content underscoring the instant participation of Mo to ODH routes and that upon increasing loading, the presence of MvK pathways is even more pronounced.

The aforementioned effects of CeO_2 content on the initial selectivity to ethylene as well as significant shift to ODH pathways over MoO_x catalysts follow the trend observed in the intensity of the 930cm^{-1} band of the fresh catalysts underscoring a plausible underlying connection. Next, we focus our efforts on investigating possible structure-reactivity relationships by coupling catalytic measurements with in-situ and Operando Raman spectroscopy.

Dynamic *in-situ* Raman Spectra of Supported MoOx Catalysts

Reduction with H_2

C-H bond activation has been shown to occur on lattice oxygen species of supported metal oxides in the Mars-van Krevelen mechanism of oxidative dehydrogenation[42, 43]. On the contrary, a metallic interaction is crucial to break C-H bonds in the direct dehydrogenation mechanism over supported metal catalysts[4]. In the present study, initial ethane conversion occurs in large part through direct participation of lattice oxygens over Mo, with the natural consequence of rapidly reducing the oxidation state of the active sites as lattice oxygen is removed. The time-on-stream dependence of the **γ** ratio presented in **Figure S7** shows that at long reaction times, the value of the **γ** ratio converged for all Mo catalysts indicating that due to deep reduction similar MoO_{x-n} surface species across samples may exist.

Dynamic Raman spectroscopy was used to investigate the effect of CeO_2 in the support on the redox properties of the dispersed active sites. The catalysts were reduced in 0.5 % H_2 at 600 °C, and the results of in-situ Raman measurements are shown in **Figure 5a-d**. Although the terminal Mo=O oxygen from molybdena species is hypothesized to be associated with non-selective combustion of ethane, changes in the intensity of this peak could still be utilized as an indicator of the overall material oxidation state. When exposed to hydrogen, the intensity of the 995 cm^{-1} peak of all materials decreased with time, signifying reduction. The Mo=O intensities shown in **Figure 5** have been normalized with respect to the initial Mo=O of the fully oxidized catalyst. We find that the reduction behavior of the Mo=O peak follows the trend P25<1CeTi<5CeTi. The spectroscopic signature of the Mo=O peak in the 5Mo/10CeTi sample could not be recorded by in-situ Raman due to its very weak intensity (discussed above) in conjunction with the very rapid rate of reduction of this catalyst. This enhancement highlights a significant improvement in reducibility of supported molybdena

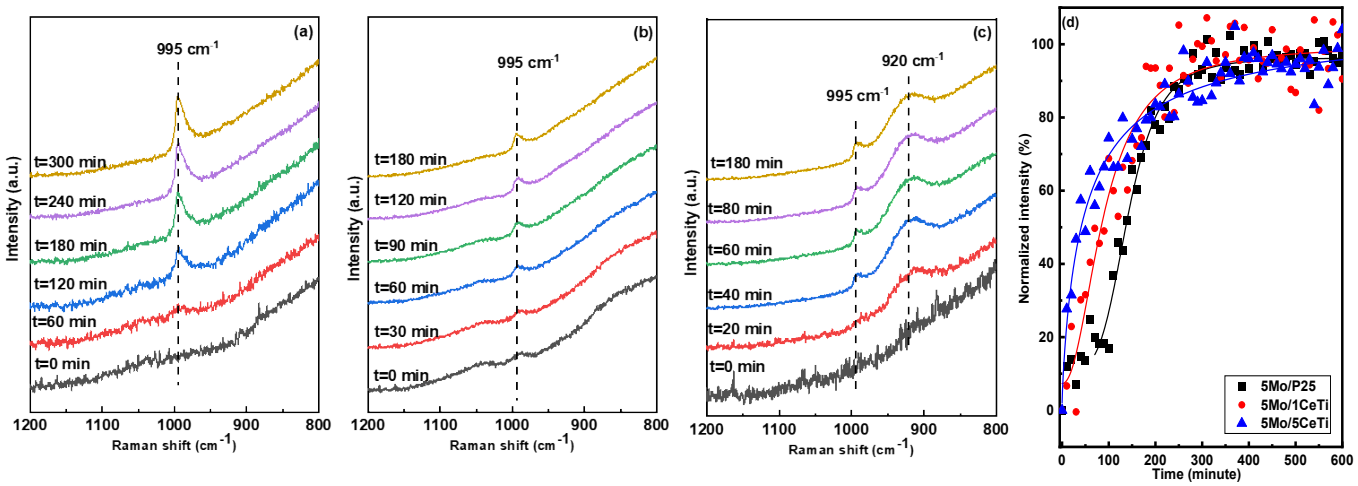

Figure 6: In-situ reoxidation at 600 °C under a 50 mL/min flow containing 60 % CO_2 and 40 % N_2 over (a) 5Mo/P25, (b) 5Mo/1CeTi, (c) 5Mo/5CeTi. (d) Analysis of the normalized Raman Mo=O intensity for the different catalysts

on mixed ceria-titania as opposed to pure P25. Our results are consistent with H_2 TPR studies showing that ceria dispersed in titania improves the reducibility of mixed oxides[29,32]. Here we show that the improvement in the redox properties of the support directly affects also the reducibility of the dispersed active phase, which in turn is expected to play a crucial role in ODH via MvK, considering that the removal of hydrogen from ethane and the release of water strongly depend on the reducibility of active sites[17, 19, 4].

Reoxidation with CO_2

Although CO_2 is utilized as a mild oxidizing agent, whether it can effectively replenish the lattice oxygen lost in the MvK mechanism, especially for the Mo catalysts, remained an open question. Considering that the rapid oxygen depletion of surface species may be responsible for the initial catalyst deactivation (**Figure S5-6**), an effort was made to understand possible reoxidation of surface species with CO_2.

An in-situ Raman study (**Figure 6**) was conducted where all catalyst were initially reduced in 0.5% H_2 and subsequently reoxidized with CO_2. After reduction, neither the peaks that correspond to the terminal (Mo=O) nor bridging (Mo–O–M, M=Mo or Support) were visible in the Raman spectra. In the presence of CO_2, both of these peaks gradually increased with time, indicating that CO_2 was indeed reoxidizing reduced surface sites. Interestingly, their intrinsic rates of reoxidation vary significantly with catalyst support. The Mo=O intensities shown in **Figure 6** have been normalized with respect to the initial Mo=O of the fully oxidized catalyst, prior to any reduction. The normalized intensity of Mo=O (**Figure 6d**) revealed that the rate of reoxidation is faster in catalysts with higher ceria content in the support. Despite this enhancement in the oxidation rate, the rate of reduction of Mo catalysts (discussed in **Figure 5d**) was still an order of magnitude faster than reoxidation by CO_2. It is worth mentioning here that for Mo catalysts with higher Ce content, i.e., 5Mo/5eTi, the intensity of the bridging bonds is recovered prior to that of the terminal. We also report that even after 200 minutes of exposure to CO_2, although the intensity of the bridging bonds is significantly recovered, its position appears to be around 920cm^{-1}, as opposed to the 930cm^{-1} in fully oxidized (with O_2) catalysts (see **Figure S9b**). Considering the highly overlapping nature of this band by different features (Mo–O–M, X=Mo or Support), we hypothesize that this red shift indicates that the CO_2 treatment may not be able to recover all the polymeric Mo domains, thus leaving smaller Mo oligomers on the catalyst surface. As the population of bridging oxygen species decreased, polymeric domains of molybnena could be expected to divide and form smaller domains. These smaller domains of polymers were less electron withdrawing at each Mo site, causing the red shift of the bridging oxygen peak[63]. The impact of this incomplete recovery (or reoxidation) by CO_2 is shown in **Figure S9b**, where catalysts were regenerated by O_2

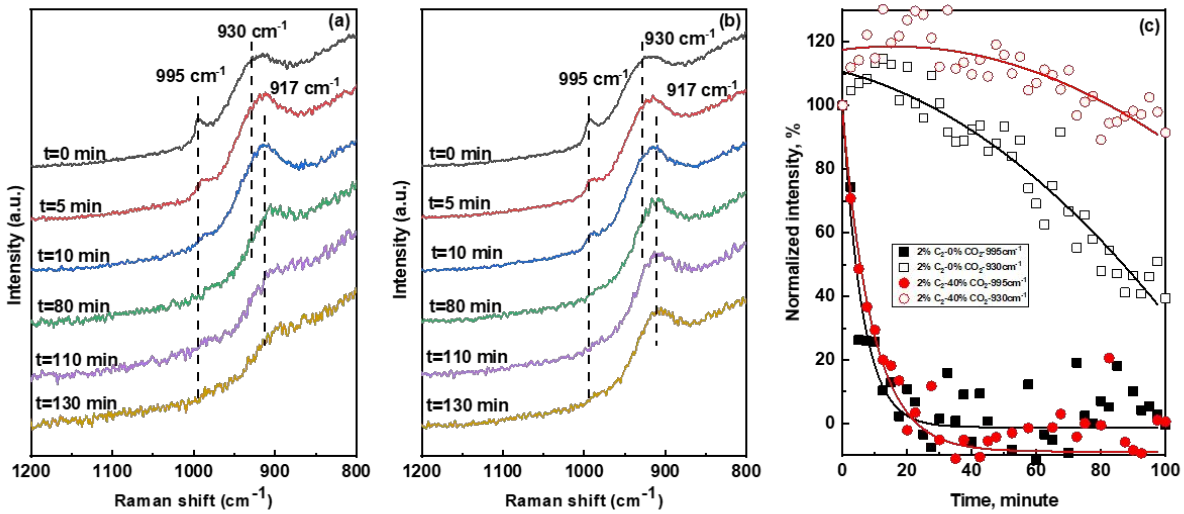

Figure 7: In-situ Raman spectra of 5Mo/5CeTi at 600°C under a 50mL/min flow containing (a) 2 % C_2H_6, and 98% N_2 (b) 2 % C_2H_6, 40 % CO_2, and 58 % N_2. (c) Change in peak intensity of molybdenyl and bridging bond during in-situ Raman spectroscopy

and by CO_2. This study showed that the catalysts could regain full activity with negligible difference after being regenerated with O_2, while regeneration with CO_2 led to only partial recovery of the original activity.

Reaction Conditions

The effect of the improved redox behavior on the spectroscopic behavior of the 5Mo/5CeTi under reaction conditions was studied next. In **Figure 7**, we compare two cases where Raman spectra in the presence of ethane, without CO_2 as well as in excess of CO_2 in the feed, were collected. In both cases, the reduction of the terminal Mo=O bond was rapid and essentially identical. Although the general trend observed was similar to that when exposed to hydrogen (**Figure 5c**) the overall reduction was slower when the reducing agent is ethane. Contrary to the Mo=O, the normalized bridging bonds appear to be significantly affected by the presence of CO_2 in the feed; when excess CO_2 was co-fed into the reactor, the bridging oxygen signal was depleted at a slower rate as oppoesed in the absence of CO_2. A red shift from 930 cm^{-1} to 920 cm^{-1} was also observed that can be associated with lower degree of polymeric MoOx species during reaction conditions.

The rapid depletion of lattice oxygen species observed by Raman spectroscopy together with the changes in the **γ** ratio with time-on-stream highlight the importance of the surface oxygen species on the ethane conversion pathways. However, it is important to mention here that the spectroscopic results of **Figure 6-7,** although they support the catalytic reactivity discussed above, provide only a qualitative trend. Future directions by means of spectrokinetics[64] where stepwise feed of reactants and simultaneous analysis of products is employed can help to provide information in a more quantitative manner. As discussed above, the catalysts could regain full activity with negligible difference after being regenerated with O_2, while regeneration with CO_2 led to only partial recovery of the original activity. As shown in the supporting information, the average carbon balance of all test reaction was approximately 98-99%. However, some carbon loss can be attributed to coke deposition. This is well justified in the presence study via post-reaction Raman characterization of all the supports and molybdena catalysts that presented in the supporting information (**Figure S9**). In almost all catalysts, Raman signatures of coke deposition are observed at 1345 cm^{-1} (D band) and at 1600 cm^{-1} (G band). However, although the neat supports present high amount of coke, the molybdena based catalysts show significantly less deposits. As shown also in **Figure 8a-d**, comparing the fresh and post-reaction 5Mo5Ce/TiO_2 catalysts, we observe that in both materials, well dispersed TiO_2 clusters with a diameter range from 5-10 nm are maintained. Across all HRTEM images we have acquired, none of CeO_2 nor MoO_3 crystalline structure have been observed, which is in line with our Raman and XRD results. After reaction, although the particle size is slightly larger than the initial state, both CeO_2 and MoO_3 crystalline structures still were not observed. Among large range of imaging area, no evidence of significant layered structure of carbon has been observed, which is also consistent with the Raman results presented in this work. Although it is also expected that any carbonaceous species will be hard to fully oxidized, we show that excess of CO_2 can help mitigate the extent of coke formation (**Figure 8B**). One cannot exclude the possibility that CO_2 might also react with the coke precursors, thus preserving longer activity of the surface species. Further studies on investigating the lifetime of catalysts in time-on-stream experiments coupled with Raman measurements can shed more light into the coke formation mechanism among different catalysts.

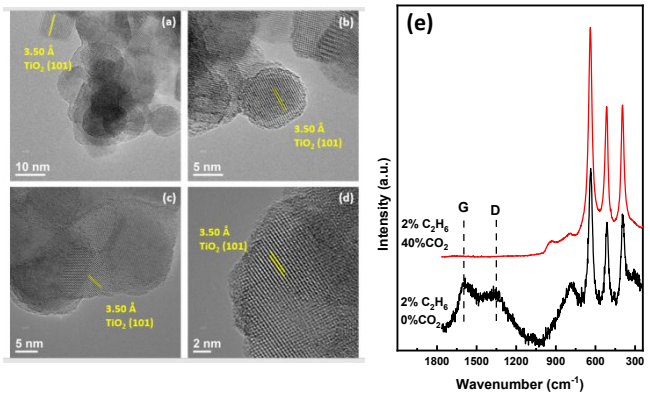

Figure 8: HRTEM images of (a), (b) fresh 5Mo/5CeTi (c), (d) post-reaction 5Mo/5CeTi. (e) Raman spectra of post-reaction over 5Mo/5CeTi under different reaction flow composition

Conclusions

Supported surface molybdena catalysts on pure P25 and mixed CeO_2-TiO_2, prepared by sol-gel method, were catalytically evaluated for the CO_2-assisted ODH of ethane. The reactivity data shown that the addition of molybdenum species enhanced the initial ethane conversion as compared to the bare supports. A maximum selectivity to ethylene of 72% was measured for the 5Mo/5CeTi catalyst. Analysis of the relative pathways for ethane conversion by means of the suggested **γ** ratio, we show that at the very early reaction time, ethylene is produced via a MvK type of mechanism while in pure supports via direct ethane dehydrogenation. At longer time-on-stream, a shift in ethane conversion pathways was observed that is associated with the depletion of reactive MoO_x sites.

Through the coupling Raman and DRIFTS characterization, it was shown that surface Mo species tend to anchor on the crystalline domains of anatase. The incorporation of ceria into the mixed oxide support improved significantly the redox properties of catalyst system. The bridging bonds, as underscored by the presence of a broad band at 930cm^{-1}, appeared to be more robust in the presence of ethane and CO_2 while the Mo=O was rapidly lost due to reduction under reaction conditions, irrespective of whether CO_2 was present. In the absence of a reducing agent, CO_2 was able to recover both the terminal and bridging molybdenum-oxygen signals in Raman (as seen also when oxidizing with O_2), but the recovery of the bridging functionalities was at a much lesser extent during reaction conditions.

Conflicts of interest

There are no conflicts to declare.

Acknowledgements

This work was conducted with funding from the RAPID manufacturing institute, supported by the Department of

Energy (DOE) Advanced Manufacturing Office (AMO), award numbers DE-EE0007888. The current RAPID project was also made possible in part by funding provided by Rutgers, The State University of New Jersey.

Notes and references

1. N. Mimura, I. Takahara, M. Inaba, M. Okamoto and K. Murata, *Catalysis Communications*, 2002, **3**, 257-262.
2. T. Ren, M. Patel and K. Blok, *Energy*, 2006, **31**, 425-451.
3. P. C. A. Bruijnincx and B. M. Weckhuysen, *Angewandte Chemie International Edition*, 2013, **52**, 11980-11987.
4. J. J. H. B. Sattler, J. Ruiz-Martinez, E. Santillan-Jimenez and B. M. Weckhuysen, *Chemical Reviews*, 2014, **114**, 10613-10653.
5. F. Solymosi, A. Oszkó, T. Bánsági and P. Tolmacsov, *The Journal of Physical Chemistry B*, 2002, **106**, 9613-9618.
6. E. Gomez, S. Kattel, B. Yan, S. Yao, P. Liu and J. G. Chen, *Nature Communications*, 2018, **9**, 1398-1398.
7. M. B. Ansari and S.-E. Park, *Energy Environ. Sci.*, 2012, **5**, 9419-9437.
8. M. D. Porosoff, M. N. Z. Myint, S. Kattel, Z. Xie, E. Gomez, P. Liu and J. G. Chen, *Angewandte Chemie International Edition*, 2015, **54**, 15501-15505.
9. Z.-J. Zhao, C.-c. Chiu and J. Gong, *Chem. Sci.*, 2015, **6**, 4403-4425.
10. T. A. Bugrova, V. V. Dutov, V. A. Svetlichnyi, V. C. Corberán and G. V. Mamontov, *Catalysis Today*, 2019, **333**, 71-80.
11. A. Christodoulakis, M. Machli, A. A. Lemonidou and S. Boghosian, *Journal of Catalysis*, 2004, **222**, 293-306.
12. Y.-M. Liu, W.-L. Feng, T.-C. Li, H.-Y. He, W.-L. Dai, W. Huang, Y. Cao and K.-N. Fan, *Journal of Catalysis*, 2006, **239**, 125-136.
13. G. Raju, B. M. Reddy and S.-E. Park, *Journal of CO2 Utilization*, 2014, **5**, 41-46.
14. G. Tsilomelekis, A. Christodoulakis and S. Boghosian, *Catalysis Today*, 2007, **127**, 139-147.
15. M. P. J. C. V. C. Guío, *Catalysis Today*, 2006, **112**, 148-152.
16. T.-q. Lei, Y.-h. Cheng, C.-x. Miao, W.-m. Hua, Y.-h. Yue and Z. Gao, *Fuel Processing Technology*, 2018, **177**, 246-254.
17. C. A. Carrero, R. Schloegl, I. E. Wachs and R. Schomaecker, *ACS Catalysis*, 2014, **4**, 3357-3380.
18. R. Koirala, R. Buechel, F. Krumeich, S. E. Pratsinis and A. Baiker, *ACS Catalysis*, 2015, **5**, 690-702.
19. K. Chen, A. T. Bell and E. Iglesia, *The Journal of Physical Chemistry B*, 2000, **104**, 1292-1299.
20. K. Chen, A. Khodakov, J. Yang, A. T. Bell and E. Iglesia, *Journal of Catalysis*, 1999, **186**, 325-333.
21. S. Deng, S. Li, H. Li and Y. Zhang, *Industrial {\&} Engineering Chemistry Research*, 2009, **48**, 7561-7566.
22. E. Nowicka, C. Reece, S. M. Althahban, K. M. H. Mohammed, S. A. Kondrat, D. J. Morgan, Q. He, D. J. Willock, S. Golunski, C. J. Kiely and G. J. Hutchings, *ACS Catalysis*, 2018, **8**, 3454-3468.
23. A. Talati, M. Haghighi and F. Rahmani, *RSC Adv.*, 2016, **6**, 44195-44204.
24. E. Gomez, B. Yan, S. Kattel and J. G. Chen, *Nature Reviews Chemistry*, 2019, **3**, 638-649.
25. D. Mukherjee, S.-E. Park and B. M. Reddy, *Journal of CO2 Utilization*, 2016, **16**, 301-312.
26. G. Dutta, U. V. Waghmare, T. Baidya, M. S. Hegde, K. R. Priolkar and P. R. Sarode, *Chemistry of Materials*, 2006, **18**, 3249-3256.
27. C. Gionco, M. C. Paganini, S. Agnoli, A. E. Reeder and E. Giamello, *Journal of Materials Chemistry A*, 2013, **1**, 10918-10926.
28. B. M. Reddy, A. Khan, Y. Yamada, T. Kobayashi, S. Loridant and J.-C. Volta, *The Journal of Physical Chemistry B*, 2003, **107**, 11475-11484.
29. Z. Shi, P. Yang, F. Tao and R. Zhou, *Chemical Engineering Journal*, 2016, **295**, 99-108.
30. J. Fang, X. Bi, D. Si, Z. Jiang and W. Huang, *Applied Surface Science*, 2007, **253**, 8952-8961.
31. B. M. Reddy, A. Khan, P. Lakshmanan, M. Aouine, S. Loridant and J.-C. Volta, *The Journal of Physical Chemistry B*, 2005, **109**, 3355-3363.
32. S. Watanabe, X. Ma and C. Song, *The Journal of Physical Chemistry C*, 2009, **113**, 14249-14257.
33. M. A. Bañares and I. E. Wachs, *Journal of Raman Spectroscopy*, 2002, **33**, 359-380.
34. C. Andriopoulou and S. Boghosian, *Phys. Chem. Chem. Phys.*, 2018, **20**, 1742-1751.
35. G. Tsilomelekis, A. Tribalis, A. G. Kalampounias, S. Boghosian, G. D. Panagiotou, K. Bourikas, C. Kordulis and A. Lycourghiotis, eds. E. M. Gaigneaux, M. Devillers, S. Hermans, P. A. Jacobs, J. A. Martens and P. Ruiz, Elsevier, 2010, vol. 175, pp. 613-616.
36. G. Busca, *Journal of Raman Spectroscopy*, 2002, **33**, 348-358.
37. H. Hu, I. E. Wachs and S. R. Bare, *The Journal of Physical Chemistry*, 1995, **99**, 10897-10910.
38. S. Xie, K. Chen, A. T. Bell and E. Iglesia, *The Journal of Physical Chemistry B*, 2000, **104**, 10059-10068.
39. G. Mestl and T. K. K. Srinivasan, *Catalysis Reviews*, 1998, **40**, 451-570.
40. G. Tsilomelekis, G. D. Panagiotou, P. Stathi, A. G. Kalampounias, K. Bourikas, C. Kordulis, Y. Deligiannakis, S. Boghosian and A. Lycourghiotis, *Phys. Chem. Chem. Phys.*, 2016, **18**, 23980-23989.
41. L. J. Burcham, J. Datka and I. E. Wachs, *The Journal of Physical Chemistry B*, 1999, **103**, 6015-6024.
42. K. Chen, S. Xie, E. Iglesia and A. T. Bell, *Journal of Catalysis*, 2000, **189**, 421-430.
43. H. Dai, A. T. Bell and E. Iglesia, *Journal of Catalysis*, 2004, **221**, 491-499.
44. H. Liu, P. Cheung and E. Iglesia, *Journal of Catalysis*, 2003, **217**, 222-232.
45. R. Radhakrishnan, C. Reed, S. T. Oyama, M. Seman, J. N. Kondo, K. Domen, Y. Ohminami and K. Asakura, *The Journal of Physical Chemistry B*, 2001, **105**, 8519-8530.
46. M. A. Vuurman and I. E. Wachs, *The Journal of Physical Chemistry*, 1992, **96**, 5008-5016.
47. I. E. Wachs, *Topics in Catalysis*, 1999, **8**, 57-63.
48. R. B. Watson and U. S. Ozkan, *Journal of Catalysis*, 2002, **208**, 124-138.
49. B. M. Weckhuysen, J.-M. Jehng and I. E. Wachs, *The Journal of Physical Chemistry B*, 2000, **104**, 7382-7387.
50. T. L. Drake and P. C. Stair, *Topics in Catalysis*, 2017, **60**, 1618-1630.
51. H. Tian, E. I. Ross and I. E. Wachs, *The Journal of Physical Chemistry B*, 2006, **110**, 9593-9600.
52. N. Doudin, G. Collinge, P. K. Gurunathan, M. S. Lee, V.-A. Glezakou, R. Rousseau and et al., *ChemRxiv Preprint*, 2020.

53. A. Badri, C. Binet and J.-C. Lavalley, *J. Chem. Soc.{\{},{\}} Faraday Trans.*, 1996, **92**, 4669-4673.
54. A. Filtschew, K. Hofmann and C. Hess, *The Journal of Physical Chemistry C*, 2016, **120**, 6694-6703.
55. H. Lin, J. Long, Q. Gu, W. Zhang, R. Ruan, Z. Li and X. Wang, *Phys. Chem. Chem. Phys.*, 2012, **14**, 9468-9474.
56. A. Mahdavi-Shakib, J. M. Arce-Ramos, R. N. Austin, T. J. Schwartz, L. C. Grabow and B. G. Frederick, *The Journal of Physical Chemistry C*, 2019, **123**, 24533-24548.
57. A. Ruiz Puigdollers, P. Schlexer, S. Tosoni and G. Pacchioni, *ACS Catalysis*, 2017, **7**, 6493-6513.
58. T. Baidya, A. Gayen, M. S. Hegde, N. Ravishankar and L. Dupont, *The Journal of Physical Chemistry B*, 2006, **110**, 5262-5272.
59. R. Zhou, Y. Cao, S.-r. Yan and K.-n. Fan, *Applied Catalysis A: General*, 2002, **236**, 103-111.
60. B. Yan, S. Yao, S. Kattel, Q. Wu, Z. Xie, E. Gomez, P. Liu, D. Su and J. G. Chen, *Proceedings of the National Academy of Sciences*, 2018, **115**, 8278-8283.
61. N. Thu D., C. Fuat E. and T. George, *CO2 Assisted Ethane Oxidative Dehydrogenation over MoO3 and V2O5 Catalysts Supported on Reducible CeO2-TiO2*, 2020.
62. H. Yan, K. He, I. A. Samek, D. Jing, M. G. Nanda, P. C. Stair and J. M. Notestein, *Science*, 2021, **371**, 1257.
63. A. Christodoulakis, E. Heracleous, A. A. Lemonidou and S. Boghosian, *Journal of Catalysis*, 2006, **242**, 16-25.
64. J. Moncada, W. R. Adams, R. Thakur, M. Julin and C. A. Carrero, *ACS Catalysis*, 2018, **8**, 8976-8986.